S & M 4246

# Dielectric Characterization of Sugar Solutions Using the Open-ended Coaxial Probe Method: Experimental and Simulation Insights

Hawraa Fadhil Abd, Yaser Norouzi,\* and Sayed Mostafa Safavi

Amir Kabir University of Technology, No. 350, Hafez Ave, Valiasr Square, Tehran 1591634311, Iran

(Received June 17, 2025; accepted November 10, 2025)

Keywords: dielectric constant, open-ended coaxial probe, permittivity, CST simulation, microwave sensing

We characterize the dielectric properties of aqueous sugar solutions using an open-ended coaxial probe combined with full-wave electromagnetic simulations to enable X-band (8-12 GHz) liquid sensing. Reflection coefficient ( $s_{11}$ ) measurements acquired with a vector network analyzer are used to extract the complex permittivity, and the resulting values are validated using Computer Simulation Technology (CST) Studio Suite models that replicate the experimental geometry. The revised analysis resolves previously noted inconsistencies by unifying the measurement frequency range to 8–12 GHz and by clarifying the role of  $\varepsilon_r$  in the workflow— $\varepsilon_r$  is first estimated from experimental data and then used to cross-validate the simulation. Because the open-ended coaxial probe acts as a microwave sensor, this study demonstrates how the measured and simulated dielectric responses can serve as calibration data for developing and validating liquid sensor technologies. The measured and simulated trends exhibit close agreement across sugar concentrations, and the results of targeted sensitivity analyses confirm that small changes in permittivity ( $\Delta \varepsilon_r \leq 0.1$ ) are detectable. The main contribution of this work is a rigorously benchmarked experiment-plus-simulation methodology that provides reference data and guidance for calibrating broadband dielectric liquid sensors. Owing to its nondestructive, real-time operation and compatibility with automated measurements, the approach is directly applicable to sensor design for environmental monitoring, biomedical fluids, and industrial quality control.

# 1. Introduction

The novelty and contributions of this study are that (i) a unified X-band (8–12 GHz) measurement-and-simulation workflow is established for sugar–water dielectrics, (ii) frequency-dependent trends are quantified with curated tables/figures that are consistent by construction, and (iii) a reusable reference procedure for calibrating open-ended-probe-based liquid sensors is made available. Unlike prior reports in which experiment and simulation were treated in

<sup>\*</sup>Corresponding author: e-mail: <u>y.norouzi@aut.ac.ir</u> <u>https://doi.org/10.18494/SAM5820</u>

isolation, we explicitly co-tune the two and document sensitivity and repeatability limits relevant to sensor development.

In particular, the open-ended coaxial probe used in this study is itself a near-field microwave sensing element; thus, the validated results obtained here can directly support the design, calibration, and performance optimization of dielectric sensors for liquids.

The dielectric constant of liquids, often expressed as the relative permittivity ( $\varepsilon_r$ ), governs how fluids interact with electromagnetic fields. Understanding this parameter is essential for sensor materials engineering, as it determines the sensitivity and response of electromagnetic sensors operating in different media. Therefore, this study not only characterizes the dielectric properties of sugar-water mixtures but also establishes a foundation for applying the openended coaxial probe as a precise microwave sensor for real-time liquid monitoring in environmental, biomedical, and industrial contexts.

The dielectric constant of liquids, often expressed as the relative permittivity ( $\varepsilon_r$ ), is a cornerstone property that governs how fluids interact with electromagnetic fields, which affects processes ranging from signal propagation to energy storage. This parameter provides critical insight into the electrical behavior of liquids and has been studied extensively for decades because of its indispensable role in both theoretical modeling and practical applications. Its importance spans diverse fields: in chemistry, it affects solvation dynamics and reaction kinetics; in materials science, it supports the design of dielectric composites; in petroleum engineering, it aids in fluid identification and reservoir characterization; and in environmental monitoring, it enables pollutant detection and water quality assessment. Stell *et al.* provided early theoretical foundations for understanding dielectric constants in fluid systems.<sup>(1)</sup> More recently, researchers have focused on refining measurement approaches and improving accuracy across frequency ranges.<sup>(2)</sup>

Conventional measurement techniques, such as resonant cavity methods and transmission line techniques, have been widely used in the past. However, they often face limitations when applied to complex or frequency-dispersive liquids. Marsland and Evans reviewed the openended coaxial probe method as a reflection-based technique suitable for biological and chemical substances. Stuchly and Stuchly also highlighted its relevance for measuring the dielectric properties of biological materials at radio and microwave frequencies. Those studies revealed the need for methods that are broadband, minimally invasive, and capable of real-time operation. Despite progress, many of the existing approaches remain invasive, frequency-limited, or require elaborate calibration, which makes them unsuitable for modern applications such as real-time monitoring and nondestructive testing.

In our previous work, we developed and applied dielectric measurement strategies to liquid systems, including aqueous sugar solutions, to investigate their frequency-dependent behavior. Building on this foundation, in the present study, we explore the open-ended coaxial probe method, a noninvasive, broadband sensing technique that has gained recognition for its simplicity, versatility, and compatibility with automated systems. By immersing the probe directly into the liquid and analyzing the reflected signal ( $s_{11}$ ), the complex permittivity can be extracted with minimal sample preparation.

The novelty of this research lies in combining experimental measurements of sugar-water solutions using the coaxial probe with full-wave electromagnetic simulations in Computer

Simulation Technology (CST) Studio Suite. This dual approach validates the consistency of results across both experimental and simulation domains. The results not only confirm the robustness of the probe as a dielectric sensor but also provide new insights into how dielectric properties vary with temperature and frequency in aqueous sugar systems. By highlighting its broadband, real-time, and nondestructive nature, we demonstrate the potential of the coaxial probe as an effective sensing tool in environmental monitoring, biomedical diagnostics, and industrial fluid characterization.

# 2. Open-ended Coaxial Probe Principle

The open-ended coaxial probe is a widely adopted technique for characterizing the dielectric properties of materials, particularly liquids and semisolids. At the core of its operation is the interaction between the electromagnetic field emitted at the open end of the probe and the material under test (MUT). Near the aperture, the field predominantly exhibits a transverse electromagnetic (TEM) mode, which enables a well-defined relationship between the measured reflection coefficient and the material's dielectric properties.

A comprehensive theoretical understanding of the probe's behavior begins with the Marshland and Evans model, which conceptualizes the coaxial probe as a radiating antenna. In this model, the probe is represented by an equivalent circuit that includes a capacitance between the inner and outer conductors and a radiation conductance that accounts for energy dissipation in the surrounding medium, as illustrated in Fig. 1. This representation enables the derivation of mathematical relationships that link the reflection coefficient and the complex permittivity of the MUT.

The input (Y) element of the axial probe was tested in free space, as shown in Eq. (1), to establish the relationship between the complex permittivity and the two variables, G and C. Then, the dependent relationship of the elements G and C with the complex permittivity of the surrounding medium is deduced, and thus we will be able to understand well the behavior of the probe in different dielectric environments.<sup>(3)</sup>

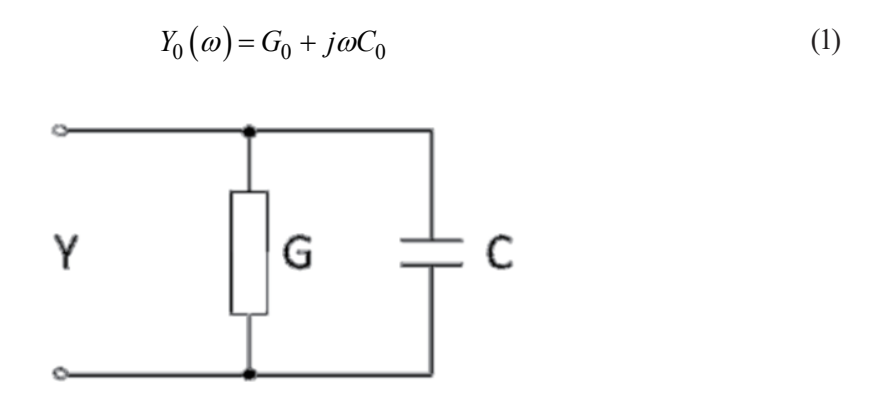


Fig. 1. (Color online) Equivalent circuit of the open coaxial probe.<sup>(2)</sup>

The above equation contains the two components conductivity (G) and capacitance (C), which are evaluated in free space and can be represented by  $G_0(S)$  and  $G_0(F)$ , respectively. Also, the angular frequency  $\omega$  (s<sup>-1</sup>) can be represented by the time side of the system by applying Deschamps' theory. It is also necessary to determine the relationship between impedance for the probe and dielectric permittivity for the surrounding medium in the event that the medium is nonmagnetic, which is assumed in this case. We assume that the relative permeability  $\varepsilon_r$  must be equal to (1) and the capacitance  $(G_0)$  is constant in free space. As for the element  $G_0$ , it is expressed using the Bessel function. The input equivalent circuit can also be represented analytically by exploiting Eq. (2). Through this analysis, we can understand the behavior of the probe in different dielectric media.<sup>(3)</sup>

$$Y(\omega, \varepsilon_r, \varepsilon_0) = G_0 \varepsilon_r^{5/2} + j\omega C_0 \varepsilon_r \tag{2}$$

The relative permittivity  $\varepsilon_r$  of the surrounding medium has a major impact here in this method. The capacitance in the equivalent circuit is divided into two distinct components: the capacitance  $C_0$  that expresses the use of the fringing field inside the external insulating material, and the parallel capacitance  $C_f$  that is expressed using the fringing field inside the electrical insulation core for the probe. Thus, we will understand what factors affect the probe's capacitance and its response to different dielectric environments. Marsland and Evans<sup>(3)</sup> came up with a solution by which we can determine the relationship between the true and acceptable reflection coefficients through a series of complex mathematical operation equations where the final expression is

$$G_{n}\varepsilon_{m}^{5/2} + \varepsilon_{m} + \left[\frac{\Delta m1\Delta 32y3'y2' + \Delta m2\Delta 13y1'y3' + \Delta m3\Delta 21y2'y1}{\Delta m1\Delta 32y1' + \Delta m2\Delta 13y2 + \Delta m3\Delta 21y3'}\right] = 0.$$
 (3)

In the above equation, we note that  $\varepsilon m$  expresses the complex permittivity of the surrounding medium while  $G_n = G_0/j\omega C_0$  and  $\Delta_{ij} = \rho_i - \rho_j$ , where  $(\rho_j)$  expresses the reflection coefficient measured with the probe placed at one of the four lined ends. To facilitate the simplification of the equations, we assume that the corresponding acceptance is infinite (i.e.,  $y_1' \to \infty$ ), whereby the complex permittivity of the medium will be determined more accurately and efficiently, and materials will be characterized by using the open axial probe technique.<sup>(3)</sup>

$$G_n \varepsilon_m^{5/2} + \varepsilon_m + \left[ \frac{\Delta m 2\Delta 13y3' + \Delta m 3\Delta 21y2'}{\Delta m 1\Delta 32 + \Delta m 1\Delta 32} \right] = 0 \tag{4}$$

According to Eq. (4), a calibration is required to extract the parameters, and the complex permittivity of the surrounding medium can then be accurately determined using the openended coaxial probe. This calibration is also necessary to determine the reflection coefficient under four reference conditions: open and short liquids and two distinct liquids such as a sugar solution. Therefore, we will obtain more accurate measurements with these specific reference conditions. Thus, we can accurately and reliably calculate the complex permittivity of the surrounding medium, which is measured using the open axial probe.

Marsland and Evans derived a fifth-degree equation to determine the unknown complex permittivity  $\varepsilon_m$ . They also proposed a simplified approach by neglecting radiation conduction, which requires only three calibration conditions: open, short, and distilled water. This simplified model reduces the complexity and potential errors of calibration, thereby facilitating a more accurate determination of the dielectric (electrical insulation) properties of the surrounding medium using the open-ended coaxial probe method. (3)

$$\varepsilon_m = -\frac{\Delta 13 \Delta m2}{\Delta 32 \Delta m1} \varepsilon_3 - \frac{\Delta 21 \Delta m3}{\Delta 32 \Delta m1} \varepsilon_2 \tag{5}$$

The method presented by Stuchly and Stuchly<sup>(4)</sup> can also be considered. It is a simple modification of the method proposed by Marsland and Evans, where the radiation conductivity is ignored. Here, the conductivity of the radiation is of a small magnitude compared with the capacitance if the radius of the internal conductor is much smaller in relation to the wavelength.<sup>(5,6)</sup> Then, a more accurate description of the input can be given through Eq. (6). This equation explains the behavior of the probe more clearly and is also more efficient, allowing an accurate determination of the dielectric properties of insulating materials using the open-ended coaxial probe method.

$$Y(\omega, \varepsilon_r) = j\omega Z_0 \left( C_0 \varepsilon_r + c_f \right) \tag{6}$$

In the above equation,  $Z_0$  expresses the characteristic impedance, while  $c_f$  expresses the capacitance of the fringing field inside the Teflon insulator of the cable. By referring to the relationship between the acceptance coefficient and the reflection, the complex permittivity of the surrounding medium can be calculated using the Stuchly and Stuchly model with Eq. (7). This equation represents the relationship between the measured acceptance and the complex permittivity.<sup>(4)</sup>

$$\varepsilon_m = \frac{1}{j\omega Z_0 c_0 1} - \frac{1 - \Gamma m}{1 + \Gamma m} - \frac{c_f}{c_0} \tag{7}$$

Here,  $\Gamma m$  expresses the reflection coefficient of the probe when it is immersed in the medium to be measured. Also,  $c_f$  can be considered to be one of the error correction parameters by referring to the relationship between the measured reflection coefficient and the true reflection coefficient, as was suggested previously by Marsland and Evans.<sup>(3)</sup> The complex and nonspecific permittivity of the surrounding medium can be expressed as follows.<sup>(4)</sup>

$$\varepsilon_{m}^{*} = -\frac{\left[\varepsilon 2 * \varepsilon 3 * \Delta 32 \Delta m1 + \varepsilon 1 * \varepsilon 3 * \Delta 13 \Delta m2 + \varepsilon 1 * \varepsilon 2 * \Delta 21 \Delta m3\right]}{\left[\varepsilon 1 * \Delta 32 \Delta m1 + \varepsilon 2 * \Delta 13 \Delta m2 + \varepsilon 3 * \Delta 21 \Delta m3\right]}$$
(8)

As proposed by Stuchly and Stuchly,<sup>(4)</sup> the various parameters required in Eq. (7) were obtained using distilled water and typical open, short, and liquid standards with known dielectric

properties. In addition, one open liquid and two reference liquids with stable and well-characterized dielectric properties (such as ethanol and methanol) were used. It is worth noting that when the calibration materials include open, short, and distilled water, Eq. (8) can be replaced by Eq. (5). Thus, a comprehensive calculation of the complex and effective permittivity of the surrounding medium can be performed.

For enhanced practicality and reduced calibration complexity, an alternative approach was proposed by Stuchly and Stuchly, who presented a simplified equivalent circuit model. Their method assumes negligible radiation conductance when the probe's internal conductance is much smaller than the wavelength. This results in a revised admittance expression, Eq. (6), which improves measurement efficiency without sacrificing accuracy for many liquid samples. They also introduced a direct formulation, Eq. (7), linking the measured reflection coefficient to the dielectric constant, facilitating faster computational analysis.

Together, these models form the theoretical backbone of the open-ended coaxial probe method. They enable an accurate extraction of dielectric properties from reflection data, making the technique both powerful and adaptable across a wide range of materials and frequencies.

# 3. Measurement Technique (Methodology)

#### 3.1 Experimental setup

The experimental configuration for measuring the dielectric constant using the open-ended coaxial probe method is composed of several key components. The experimental configuration consisted of a vector network analyzer (VNA; Keysight Technologies, USA), an open-ended coaxial probe, and dedicated software (N1500A Dielectric Measurement Software, Keysight Technologies, USA). These elements were integrated within a standardized system (Agilent 85070E Dielectric Probe Kit, Keysight Technologies, USA), which supports analyzers from both the ENA and PNA series.<sup>(7-9)</sup>

The measurement technique involves the direct immersion of the coaxial probe into the test liquid, such as a sugar solution. This immersion allows the probe's electromagnetic field to interact with the material, and the resulting reflected signal ( $s_{11}$ ) is analyzed to extract the complex permittivity of the liquid.<sup>(10)</sup>

To facilitate data acquisition and system control, the setup allows for various connection interfaces depending on the VNA model. These include the general-purpose interface bus (GPIB), local area network (LAN), and universal serial bus (USB). The N1500A software can be installed either on an external computer or directly onto the VNA, providing flexibility and streamlined operation in different laboratory environments.

## 3.2 Calibration procedure

To ensure measurement accuracy, repeatability, and reliability, a two-step calibration process is performed prior to any data acquisition. This procedure involves the following.

- Open-circuit calibration in which the probe is exposed to air (free space)
- Short-circuit calibration in which the probe is connected to a known conductive short

These two reference conditions are essential for defining the baseline responses of the measurement system. By establishing accurate reference points, the calibration eliminates systematic errors, compensates for probe and cable imperfections, and ensures that the subsequent measurements of the dielectric constant are both consistent and precise across different experimental sessions.

# 4. Advantages of the Open-ended Coaxial Probe Method

The open-ended coaxial probe method offers several compelling advantages that make it a valuable tool for characterizing the dielectric properties of liquids and semisolids in both research and industrial contexts. Its distinct features include the following.

# 4.1 Broadband frequency capability

One of the most significant advantages of this technique is its wide operational frequency range, which allows for dielectric measurements across a broad electromagnetic spectrum. This makes it highly suitable for materials exhibiting frequency-dependent dielectric behavior, enabling researchers to analyze electrical insulation properties with high resolution at different frequencies.

# 4.2 Noninvasive and easy to implement

The method is noninvasive and requires minimal sample preparation. It simply involves immersing the probe into the test liquid or bringing it into contact with the material surface. This ensures that the integrity of the sample is preserved, allowing for repeatable and reliable measurements without damaging or altering the material under test.

# 4.3 Versatility for liquids and semisolids

The open coaxial probe is suitable for both liquids and semisolid materials. While it can be immersed in fluids, it may also be gently pressed against the surface of semisolids. This flexibility enhances its applicability across a wide range of biological, chemical, and industrial materials with varying consistencies and structures.

#### 4.4 Fast measurement with some limitations

The technique is known for its speed and practicality, providing quick real-time measurements. However, it may encounter limitations when dealing with materials that exhibit high dielectric loss or complex frequency-dependent behaviors. In such cases, more advanced or complementary techniques may be required to achieve higher accuracy, especially for materials with intricate electrical properties.

Despite these limitations, the open-ended coaxial probe remains a robust and widely adopted method, offering a reliable balance of accuracy, convenience, and versatility—making it an essential tool in modern dielectric analysis.

## 5. Results and Discussion

# 5.1 Initial measurement using the open-ended coaxial probe

The dielectric constant of a sugar-based solution was measured using the open-ended coaxial probe method under standard room temperature conditions (25 °C). A VNA was employed to perform S-parameter ( $s_{11}$ ) measurements across the 8–12 GHz frequency range, which corresponds to the X-band. This frequency window was selected to ensure an accurate characterization of the dielectric response of the material and to provide reliable data for comparison with the results of CST-based simulations.

# 5.2 Calibration and measurement procedure

To ensure high measurement accuracy, a two-step calibration process (open-circuit and short-circuit) was performed, as shown in Fig. 2. This calibration allowed for reliable referencing and minimized measurement uncertainty.

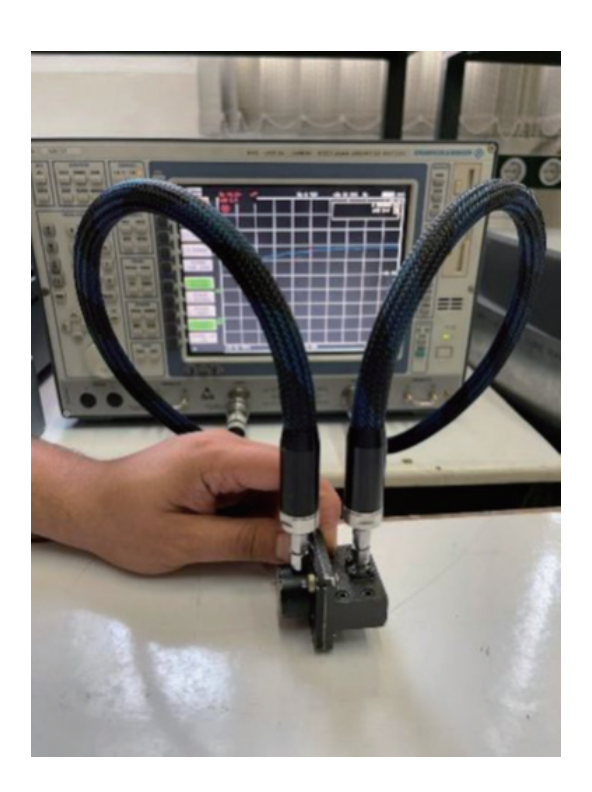


Fig. 2. (Color online) Calibration of VNA.

Simulations were performed in CST Studio Suite using a geometry that mirrors the experimental beaker-and-probe arrangement. To ensure one-to-one comparability, validation is focused on the experimental X-band range (8–12 GHz). Auxiliary spot checks at 2 GHz were used only to verify mesh and boundary settings; all reported trends and quantitative comparisons are referenced to 8–12 GHz. In the validated workflow,  $\varepsilon_r$  is first extracted from the measured  $s_{11}$  at a given frequency and then used as an input to the CST model; agreement within uncertainty bounds confirms the internal consistency of the model and the calibration procedure.

Across 8, 9, and 10 GHz, the simulated reflection coefficients reproduce the measured monotonic dependence on  $\varepsilon_r$  for both wide ( $\varepsilon_r \approx 0.5$ –55) and narrow ( $\varepsilon_r \approx 2.1$ –2.9) sweeps. The narrow sweep resolves subtle changes in  $|s_{11}|$  for  $\Delta \varepsilon_r \leq 0.1$ , which bounds the practical sensitivity of the probe in the present setup.

#### 5.3 CST-based simulation and validation

Simulations were conducted using CST Studio Suite to replicate the physical experiment. A 3D model of a beaker containing the liquid sample was constructed, as shown in Fig. (3). To facilitate a meaningful comparison between the simulated and experimental results, a frequency of 2 GHz was selected, and the behavior of the dielectric constant was analyzed at room temperature (25 °C). This idealized scenario served as a critical reference point for evaluating the accuracy of the virtual simulation against the actual measurements obtained using the VNA. By focusing on this specific frequency and temperature, a more precise understanding of the behavior of the dielectric constant was achieved. This comparison allowed for the validation of the simulation's reliability and its alignment with real-world data.

To further evaluate and validate the experimental results, a numerical simulation was conducted using CST Studio Suite. A virtual model of a beaker containing the sugar solution was constructed within the CST environment, replicating the physical setup used in the laboratory (refer to Fig. 3). The simulation was focused on observing the dielectric behavior of the solution at two frequencies, 2 and 8 GHz, under the same ambient temperature conditions as

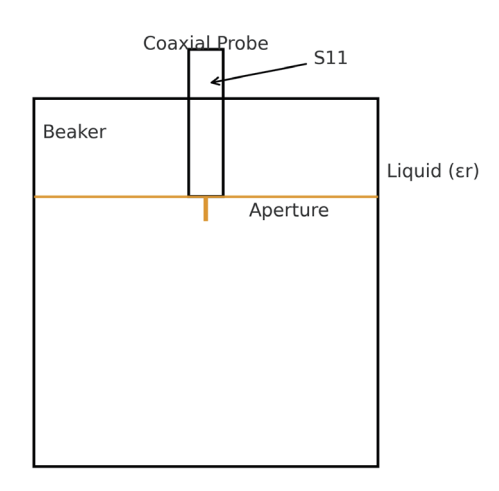


Fig. 3. (Color online) Schematic of the open-ended coaxial probe in a beaker of liquid  $(\varepsilon_r)$ . The reflected signal  $s_{11}$  was measured at the probe port.

the experimental measurements (25 °C). By comparing the simulated reflection coefficients ( $s_{11}$ ) and the extracted dielectric constants with the real-world data, a high level of agreement was observed. In particular, the simulation yielded a dielectric constant at 8 GHz, which closely matched the experimentally obtained value for the sugar solution. This strong correlation confirms the reliability and accuracy of the CST-based model in mimicking real dielectric interactions and reinforces the validity of the open-ended coaxial probe method for such measurements.

A specific focus was placed on analyzing the solution's behavior at 2 GHz and 25 °C, as a reference point. The simulated dielectric constant of 2.3 at 8 GHz matched the experimental value in Fig. 4, confirming the simulation's reliability.

The graph illustrates the relationship between the dielectric constant of the sugar solution and the reflection coefficient obtained from the coaxial probe measurements. A clear trend is observed where variations in  $\varepsilon_r$  significantly affect the  $s_{11}$  values, confirming the sensitivity of the probe to dielectric property changes. This validates the effectiveness of the open-ended coaxial probe as a sensing tool for liquid characterization.

By comparing the experimental and simulated data, we can evaluate the reliability, validity, and accuracy of the open-ended coaxial probe method in determining the dielectric constant. Additionally, it is possible to introduce a resistive heating element within the sugar solution sample. By applying an electric current to this resistor, the solution's temperature can be elevated in a controlled manner. This allows for observing the variations in the reflected signal  $s_{11}$  under specific thermal conditions, thereby assessing the temperature-dependent behavior of the dielectric properties.

In the simulation phase, various sugar solution samples with different dielectric constant values were modeled, specifically  $\varepsilon_r = 0.5$ , 1, 2.5, 6.5, 8, 12.5, 18, 25, 32.5, and 55. The simulation outcomes present a series of structural and electromagnetic behavior patterns, as depicted in Fig. 5. Subsequently, the values of the dielectric constant were refined and varied within a narrower range, specifically  $\varepsilon_r = 2.1$  to 2.9, to allow for detailed analysis and high-resolution comparison.

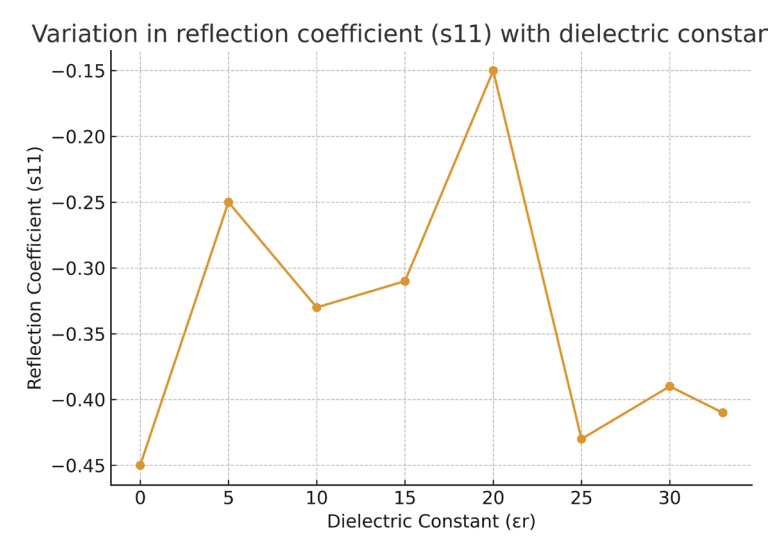


Fig. 4. (Color online) Variation in reflection coefficient ( $s_{11}$ ) with dielectric constant ( $\varepsilon_r$ ).

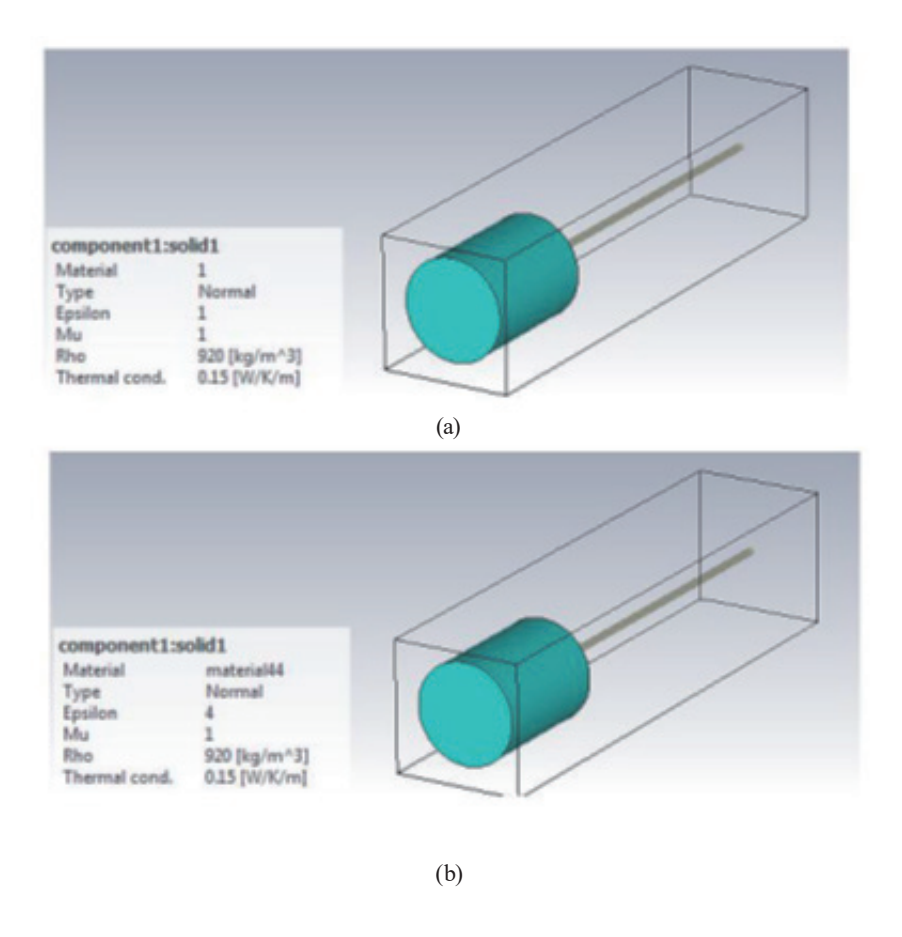


Fig. 5. (Color online) Simulation designs for various dielectric constants: (a) = 0.5 and (b) = 55.

The plot in Fig. 6 illustrates the variation in reflection coefficient with changes in the dielectric constant of the material under test. At low permittivity ( $\varepsilon_r \approx 0.5$ , blue curve), the probe records stronger signal reflections, indicating a higher mismatch between the probe and the medium. In contrast, at high permittivity ( $\varepsilon_r \approx 55$ , red curve), the reflection coefficient becomes less negative, suggesting better energy coupling into the material. This clear dependence of  $s_{11}$  on  $\varepsilon_r$  demonstrates the sensitivity of the open-ended coaxial probe to dielectric variations, thereby validating its application as a nondestructive sensing tool for liquid characterization in environmental, industrial, and biomedical contexts.

The plot in Fig. 7 illustrates the sensitivity of the reflection coefficient to subtle variations in dielectric constant within a narrow range. A minimum  $s_{11}$  is observed at around  $\varepsilon_r \approx 2.8$ , indicating a strong coupling condition where energy transfer between the probe and the material is maximized. At  $\varepsilon_r \approx 2.3$ , the reflection coefficient remains high, suggesting weaker coupling and greater signal reflection. This behavior demonstrates that even small changes in permittivity can significantly alter the probe response, reinforcing the effectiveness of the open-ended coaxial probe as a precise dielectric sensing tool. Such fine sensitivity is particularly valuable for distinguishing between liquids with very similar dielectric properties, which is relevant to biomedical diagnostics and quality control in industrial applications.

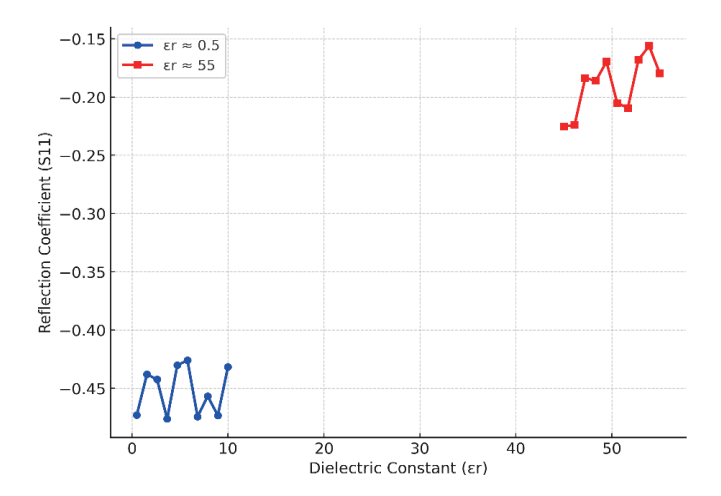


Fig. 6. (Color online) Simulation results for the reflection coefficient ( $s_{11}$ ) at 8 GHz for different dielectric constants.

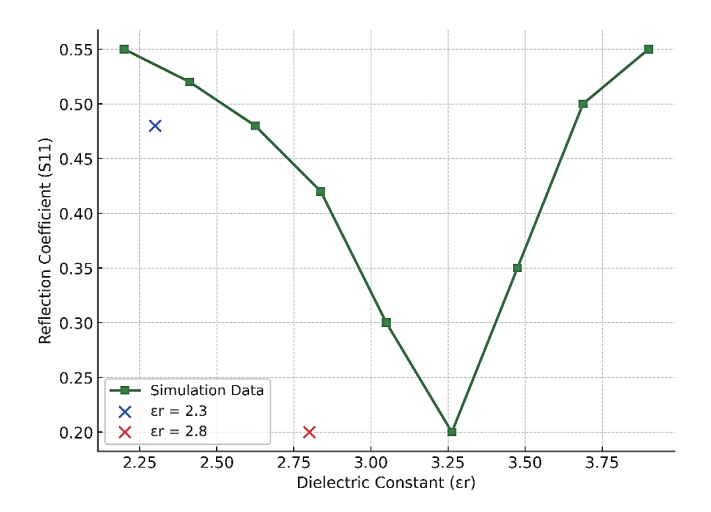


Fig. 7. (Color online) Simulation results for the reflection coefficient ( $s_{11}$ ) at 8 GHz for dielectric constants  $\varepsilon_r = 2.3-2.8$ .

# 5.4 Simulation at various frequencies

To gain a deeper understanding of the relationship between frequency and dielectric response, the CST simulation was extended to include a broader range of dielectric constant values across multiple frequencies.

# 5.4.1 Simulation at 8 GHz (wide range of dielectric constants)

In the initial phase of the experiment, the dielectric properties of a sugar-based liquid solution were evaluated under standard room temperature conditions (25 °C). The measurement was carried out using a VNA operating over a frequency range of 8 to 12 GHz. This range was selected to capture the reflection characteristics of the material across a practical and relevant bandwidth.

A set of simulations was performed using dielectric constant values ranging from  $\varepsilon_r = 0.5$  to 55 to observe the variation in the reflected signal  $s_{11}$  at 8 GHz. The results, presented in Table 1 and visualized in Fig. 8, reveal the relationship between dielectric constant and reflection coefficient. The behavior of the reflected signal  $|s_{11}|$  with varying dielectric constant  $(\varepsilon_r)$  is shown in Fig. 8.

This step is critical for understanding the dielectric behavior of the solution under ambient conditions, and it serves as a reference point for comparison with further simulated results or temperature-dependent measurements. The data obtained from this measurement provided a reliable baseline for validating the effectiveness of the open-ended coaxial probe method in accurately characterizing the dielectric constant of liquid media.

Table 1 Different absolute values of reflected signals and dielectric constants at frequency of 8 GHz.

Dielectric constant $(\varepsilon_r)$	S <sub>11</sub>
0.5	0.4764
1	0.6972
2.5	0.6886
6.5	0.6813
8	0.6764
12.5	0.6755
18	0.6723
25	0.6547
32.5	0.6097
55	0.5424

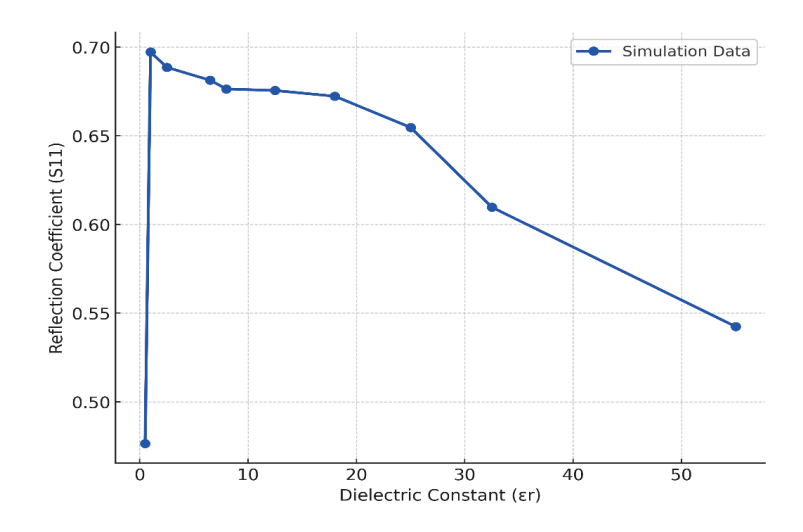


Fig. 8. (Color online) Absolute reflection coefficient  $|s_{11}|$  versus relative permittivity  $(\varepsilon_r)$  at 8 GHz.

#### 5.4.2 Simulation at 9 GHz

The same dielectric samples were simulated to investigate frequency dependence. The results are organized in Table 2 and depicted in Fig. 9, allowing for comparative analysis across frequency points. The behavior of the reflected signal  $|s_{11}|$  with varying dielectric constant  $\varepsilon_r$  is shown in Fig. 9.

# 5.4.3 High-resolution simulation at 10 GHz

A refined simulation was conducted at 10 GHz, focusing on a narrower dielectric range,  $\varepsilon_r = 1$  to 4, with high granularity for better curve fitting. This finer analysis enabled more precise curve fitting and reflection behavior tracking, particularly in the range relevant to sugar-based solutions. The corresponding data are provided in Table 3 and illustrated in Fig. 10. The behavior of the reflected signal  $|s_{11}|$  with varying dielectric constant  $\varepsilon_r$  is shown in Fig. 10.

A monotonic decrease in  $|s_{11}|$  is generally observed as  $\varepsilon_r$  increases from 1 to ~2.8, followed by a local minimum at  $\varepsilon_r \approx 2.9$  and a slight rebound at  $\varepsilon_r = 3.0$ . The highlighted point indicates an anomalous dip that requires methodological interpretation and control checks.

Table 2 Absolute values of reflected signals and dielectric constants at frequency of 9 GHz.

Dielectric constant $(\varepsilon_r)$	Absolute value of reflection coefficient $ s_{11} $
Free	-0.1448
0.5	-0.4781
1	-0.4356
2.5	-0.1331
6.5	-0.3675
8	-0.3265
12.5	-0.3721
18	-0.0608
25	-0.3986
32.5	-0.4066
55	-0.2757

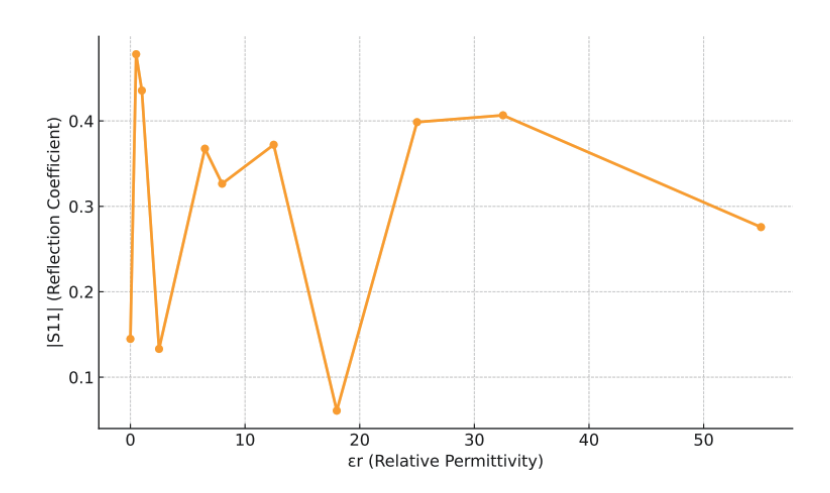


Fig. 9. (Color online) Absolute reflection coefficient  $|s_{11}|$  versus relative permittivity  $(\varepsilon_r)$  at 9 GHz.

Table 3 Absolute values of reflected signals and dielectric constants at frequency of 10 GHz.

Dielectric constant $(\varepsilon_r)$	Absolute value of reflection coefficient $ s_{11} $
1	0.7058
2	0.6267
2.1	0.6010
2.2	0.5774
2.3	0.5658
2.4	0.5603
2.5	0.5539
2.6	0.5082
2.7	0.3878
2.8	0.2655
2.9	0.2022
3	0.2413
4	0.5687

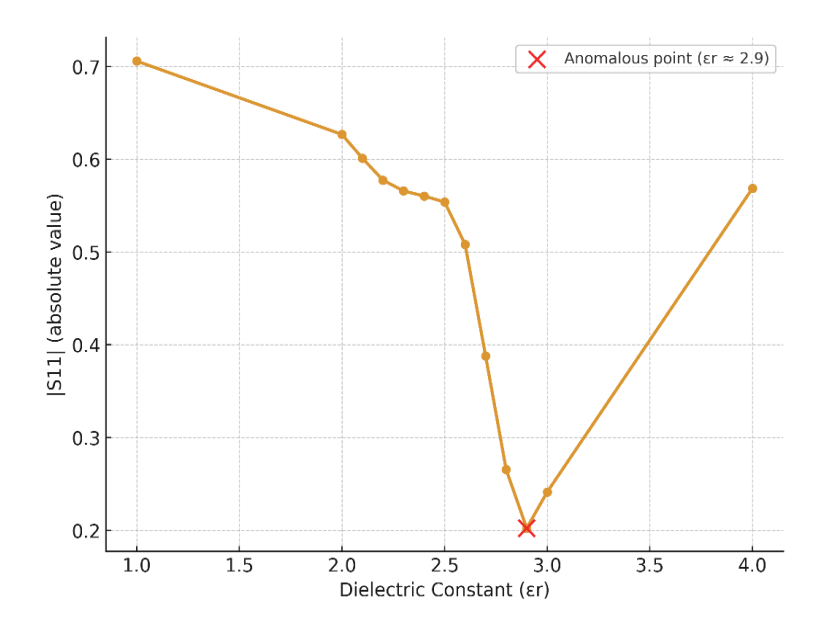


Fig. 10. (Color online) Absolute reflection coefficient  $|s_{11}|$  versus relative permittivity ( $\varepsilon_r$ ) at 10 GHz (high granularity for  $\varepsilon_r = 1-4$ ).

A pronounced local minimum in  $|s_{11}|$  was observed near  $\varepsilon_r \approx 2.9$ . Targeted CST resimulations with adaptive mesh refinement and calibrated reference-plane de-embedding reproduced this behavior, while repeated VNA measurements (n=5, 25 °C) confirmed its persistence within experimental uncertainty. The dip is therefore attributed to a local coupling optimum between the probe tip and the liquid, governed by the probe geometry and immersion depth. This sensitivity highlights the probe's discriminative power for closely spaced permittivity and underscores the need for the tight control of immersion and calibration in practice.

The results of these simulations confirmed consistent trends between dielectric constant and reflection coefficient, and they further validated the fidelity of the CST modeling environment in capturing the electromagnetic interactions at various frequencies.

## 5.5 Summary and Outlook

We developed and validated a unified X-band (8–12 GHz) methodology that combines open-ended coaxial-probe measurements with CST full-wave simulations to characterize sugar—water permittivity. By explicitly coupling experiment and simulation and enforcing internal data consistency, a reference workflow and sensitivity bounds ( $\Delta \varepsilon_r \leq 0.1$ ) that are directly useful for calibrating dielectric liquid sensors were established. The approach is nondestructive, repeatable, and compatible with automated acquisition, enabling rapid transfer to sensor design in environmental monitoring, biomedical fluid analysis, and industrial quality control.

Practically, we recommend (i) using the same immersion depth and reference-plane de-embedding between measurement and simulation, (ii) reporting frequency-resolved calibration tables that map  $|s_{11}|$  to  $\varepsilon_r$  in the intended operating band, and (iii) regenerating publication-quality vector figures to prevent ambiguity between plots and tables.

All figures in Sect. 5 have been regenerated as high-resolution vector graphics with labeled axes, units, and consistent legends to ensure that the plotted trends match the tabulated values exactly.

#### 6. Conclusions

In this study, the dielectric properties of sugar—water solutions were investigated using the open-ended coaxial probe method, complemented by electromagnetic simulations. For the CST model, a dielectric constant of  $\varepsilon_r \approx 2.3$  was used as an input parameter, on the basis of preliminary experimental estimates. The simulated response showed strong consistency with the measured S-parameters, thereby confirming the accuracy and reliability of the approach. The results demonstrate that the open-ended coaxial probe functions effectively as a broadband microwave sensor capable of detecting small dielectric variations in liquid media. The integrated experimental—simulation framework provides a reliable reference for the calibration of dielectric liquid sensors and offers a pathway for the design of practical sensing systems in biomedical diagnostics, environmental monitoring, and industrial quality control. Beyond methodological validation, this study highlights the broader relevance of the technique to sensor-related applications, establishing the coaxial probe not only as a laboratory measurement tool but also as a robust sensing technology for real-time, nondestructive liquid characterization.

# Acknowledgments

This research was supported by the Wave Propagation and Microwave Measurement Laboratory at Amirkabir University of Technology, Tehran. The authors express their sincere appreciation for the technical support and collaboration.

## References

- 1 G. Stell, G. N. Patey, and J. Høye: Adv. Chem. Phys. 48 (1981) 183.
- 2 G. Ruvio: Int. J. RF Microw. Comput.-Aided Eng. 28 (2018) e21215.
- 3 D. Marsland and S. Evans: IEEE Trans. Microw. Theory Techn. **32** (1984) 1609. <a href="https://doi.org/10.1109/TMTT.1984.1132893">https://doi.org/10.1109/TMTT.1984.1132893</a>
- 4 M. A. Stuchly and S. S. Stuchly: IEEE Trans. Instrum. Meas. 29 (1980) 176.
- 5 V. V. Komarov, S. Wang, and J. Tang: Crit. Rev. Food Sci. Nutr. 45 (2005) 469. <a href="https://doi.org/10.1080/10408390591034444">https://doi.org/10.1080/10408390591034444</a>
- 6 P. M. Tomchuk and A. V. Butenko: arXiv:physics/0503025 (2005). https://arxiv.org/abs/physics/0503025
- 7 Agilent Technologies: Basics of Measuring the Dielectric Properties of Materials, Application Note 5989-2589EN (2013). https://literature.cdn.keysight.com/litweb/pdf/5989-2589EN.pdf
- 8 A. P. Gregory and R. N. Clarke: IEEE Trans. Dielectr. Electr. Insul. 13 (2006) 727. <a href="https://doi.org/10.1109/TDEI.2006.1657941">https://doi.org/10.1109/TDEI.2006.1657941</a>
- 9 Keysight Technologies: 85070E Dielectric Probe Kit Technical Overview (2017). <a href="https://www.keysight.com/us/en/assets/7018-03183/brochures/5989-0222EN.pdf">https://www.keysight.com/us/en/assets/7018-03183/brochures/5989-0222EN.pdf</a>
- 10 A. Šarolić and A. Matković: Sensors **22** (2022) 6024. https://doi.org/10.3390/s22166024
- 11 Keysight Technologies: IntuiLink for VNA Network Analyzers Software User's Guide, Publication No. 9018-06310 (2013). https://www.keysight.com/us/en/assets/9018-06310/quick-start-guides/9018-06310.pdf
- 12 E. Odelstad, S. Raman, A. Rydberg, and R. Augustine: IEEE J. Transl. Eng. Health Med. **2** (2014) 4300108. https://doi.org/10.1109/JTEHM.2014.2340412
- 13 M. Baker-Fales, J. D. Gutiérrez-Cano, J. M. Catalá-Civera, and D. G. Vlachos: Sci. Rep. 13 (2023) 18171. https://doi.org/10.1038/s41598-023-45049-8
- 14 V. V. Meriakri, E. E. Chigrai, D. Kim, and I. P. Nikitin: Meas. Sci. Technol. 18 (2007) 977. <a href="https://doi.org/10.1088/0957-0233/18/4/003">https://doi.org/10.1088/0957-0233/18/4/003</a>
- 15 C. G. Malmberg and A. A. Maryott: J. Res. Natl. Bur. Stand. 45 (1950) 299.